



## Sparse decomposition light-field microscopy for high speed imaging of neuronal activity: supplement

**YOUNG-GYU YOON,<sup>1,2,3,4,†</sup> ZEGUAN WANG,<sup>2,5,†</sup>  NIKITA PAK,<sup>2,6</sup> DEMIAN PARK,<sup>2</sup> PEILUN DAI,<sup>2,7,8</sup> JEONG SEUK KANG,<sup>2,9</sup> HO-JUN SUK,<sup>2,10</sup> PANAGIOTIS SYMVOULIDIS,<sup>2</sup>  BURCU GUNER-ATAMAN,<sup>2</sup> KAI WANG,<sup>11,12,13,18</sup> AND EDWARD S. BOYDEN<sup>2,7,14,15,16,17,\*</sup>**

<sup>1</sup>Department of Electrical Engineering and Computer Science, Massachusetts Institute of Technology (MIT), Cambridge, Massachusetts 02139, USA

<sup>2</sup>MIT Center for Neurobiological Engineering, Massachusetts Institute of Technology (MIT), Cambridge, Massachusetts 02139, USA

<sup>3</sup>School of Electrical Engineering, KAIST, Daejeon, Republic of Korea

<sup>4</sup>KAIST Institute for Health Science and Technology, Daejeon, Republic of Korea

<sup>5</sup>School of Physical Sciences, University of Science and Technology of China, Hefei, China

<sup>6</sup>Department of Mechanical Engineering, Massachusetts Institute of Technology (MIT), Cambridge, Massachusetts 02139, USA

<sup>7</sup>Department of Brain and Cognitive Sciences, Massachusetts Institute of Technology (MIT), Cambridge, Massachusetts 02139, USA

<sup>8</sup>Department of Computer Science, Boston University, Boston, Massachusetts 02215, USA

<sup>9</sup>John A. Paulson School of Engineering and Applied Sciences, Harvard University, Cambridge, Massachusetts 02138, USA

<sup>10</sup>Harvard-MIT Health Sciences and Technology, Massachusetts Institute of Technology (MIT), Cambridge, Massachusetts 02139, USA

<sup>11</sup>Institute of Neuroscience, State Key Laboratory of Neuroscience, CAS Center for Excellence in Brain Science and Intelligence Technology, Shanghai Institutes for Biological Sciences, Chinese Academy of Sciences, Shanghai, China

<sup>12</sup>University of Chinese Academy of Sciences, Beijing, China

<sup>13</sup>Shanghai Center for Brain Science and Brain-Inspired Intelligence Technology, Shanghai, China

<sup>14</sup>Department of Biological Engineering, Massachusetts Institute of Technology (MIT), Cambridge, Massachusetts 02139, USA

<sup>15</sup>McGovern Institute for Brain Research, Massachusetts Institute of Technology (MIT), Cambridge, Massachusetts 02139, USA

<sup>16</sup>Koch Institute for Integrative Cancer Research, Massachusetts Institute of Technology (MIT), Cambridge, Massachusetts 02139, USA

<sup>17</sup>Department of Media Arts and Sciences, Massachusetts Institute of Technology (MIT), Cambridge, Massachusetts 02139, USA

<sup>18</sup>e-mail: wangkai@ion.ac.cn

\*Corresponding author: [edboyden@mit.edu](mailto:edboyden@mit.edu)

<sup>†</sup>These authors contributed equally to this paper.

---

This supplement published with The Optical Society on 20 October 2020 by The Authors under the terms of the [Creative Commons Attribution 4.0 License](https://creativecommons.org/licenses/by/4.0/) in the format provided by the authors and unedited. Further distribution of this work must maintain attribution to the author(s) and the published article's title, journal citation, and DOI.

Supplement DOI: <https://doi.org/10.6084/m9.figshare.12962678>

# Sparse decomposition light-field microscopy for high speed imaging of neuronal activity: supplementary material

YOUNG-GYU YOON,<sup>1,2,3,4,\*</sup> ZEGUAN WANG,<sup>2,5,\*</sup> NIKITA PAK,<sup>2,6</sup> DEMIAN PARK,<sup>2,7,8</sup>  
 PEILUN DAI,<sup>2,7,8</sup> JEONG SEUK KANG,<sup>2,9</sup> HO-JUN SUK,<sup>2,10</sup> PANAGIOTIS  
 SYMVOULIDIS,<sup>2</sup> BURCU GUNER-ATAMAN,<sup>2</sup> KAI WANG,<sup>11,12,13,\*\*</sup> EDWARD S.  
 BOYDEN<sup>2,7,14,15,16,17,\*\*</sup>

<sup>1</sup>Department of Electrical Engineering and Computer Science, Massachusetts Institute of Technology (MIT), Cambridge, MA, USA

<sup>2</sup>MIT Center for Neurobiological Engineering, Massachusetts Institute of Technology (MIT), Cambridge, MA, USA<sup>3</sup>

<sup>3</sup>School of Electrical Engineering, KAIST, Daejeon, Republic of Korea

<sup>4</sup>KAIST Institute for Health Science and Technology, Daejeon, Republic of Korea

<sup>5</sup>School of Physical Sciences, University of Science and Technology of China, Hefei, China

<sup>6</sup>Department of Mechanical Engineering, Massachusetts Institute of Technology (MIT), Cambridge, MA, USA

<sup>7</sup>Department of Brain of Cognitive Sciences, Massachusetts Institute of Technology (MIT), Cambridge, MA, USA

<sup>8</sup>Department of Computer Science, Boston University, Boston, MA, USA

<sup>9</sup>John A. Paulson School of Engineering and Applied Sciences, Harvard University, Cambridge, Massachusetts, USA

<sup>10</sup>Harvard-MIT Health Sciences and Technology, Massachusetts Institute of Technology (MIT), Cambridge, MA, USA

<sup>11</sup>Institute of Neuroscience, State Key Laboratory of Neuroscience, CAS Center for Excellence in Brain Science and Intelligence Technology, Shanghai Institutes for Biological Sciences, Chinese Academy of Sciences, Shanghai, China

<sup>12</sup>University of Chinese Academy of Sciences, Beijing, China

<sup>13</sup>Shanghai Center for Brain Science and Brain-Inspired Intelligence Technology, Shanghai, China.

<sup>14</sup>Department of Biological Engineering, Massachusetts Institute of Technology (MIT), Cambridge, MA, USA

<sup>15</sup>McGovern Institute for Brain Research, Massachusetts Institute of Technology (MIT), Cambridge, MA, USA

<sup>16</sup>Koch Institute for Integrative Cancer Research, Massachusetts Institute of Technology (MIT), Cambridge, MA, USA

<sup>17</sup>Department of Media Arts and Sciences, Massachusetts Institute of Technology (MIT), Cambridge, MA, USA

\*These authors contributed equally to this work.

\*\*Corresponding author: [wangkai@ion.ac.cn](mailto:wangkai@ion.ac.cn), [edboyden@mit.edu](mailto:edboyden@mit.edu)

---

This document provides supplementary information to “Sparse decomposition light-field microscopy for high speed imaging of neuronal activity,” <https://doi.org/10.1364/OPTICA.392805>. Supplementary figures and tables are included to demonstrate extended results and detailed methods for the experiments. In addition, the captions for the media that contain functional imaging results are included.

---

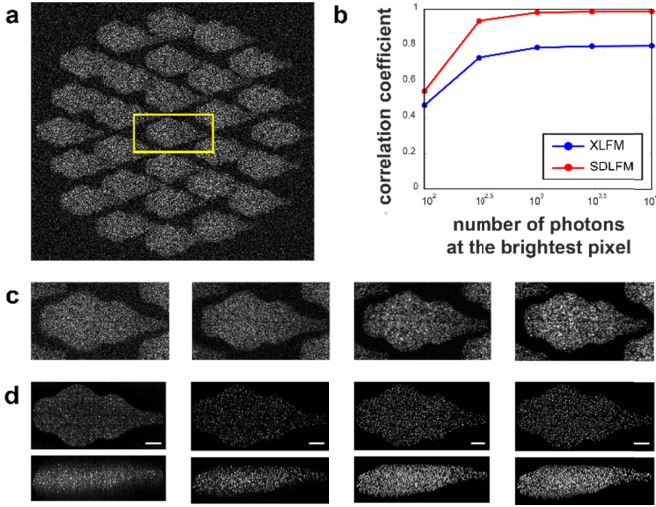


**Fig. S1.** SDLFM simulation with varying level of noise. (a) A simulated SDLFM image of a zebrafish brain acquired with the brightness level of 100 photons, captured at the brightest pixel. The magnified view of the yellow boxed region is shown in c. (b) Median values of correlation coefficients obtained by comparing the ground truth and the extracted activity from simulated XLFM (blue) and SDLFM (red) images with brightness levels of 100, 300, 1000 and 3000 photons captured at the brightest pixel (from left to right). 6.3 percent of the neurons were simultaneously active in each frame. (c) The magnified views of the yellow boxed region in a with brightness levels of 100, 300, 1000 and 3000 photons captured at the brightest pixel (from left to right). (d) Maximum intensity projections of the reconstructed volumes with brightness levels of 100, 300, 1000 and 3000 photons captured at the brightest pixel (from left to right). Top, axial projections. Bottom, lateral projections. Scale bar, 100  $\mu\text{m}$ .

the intensity profile in c. From the same raw data as in a. Scale bar, 100 $\mu\text{m}$ . (c) Magnified spatial MIP views of the yellow boxed region in b from a single frame (rather than a temporal MIP) and the lateral and axial intensity profiles across the yellow dashed lines. Within the MIP images on the left side, top left, axial projection, top right, rostral-caudal projection, bottom, lateral projection. Scale bar, 10  $\mu\text{m}$ . A.U., arbitrary units.

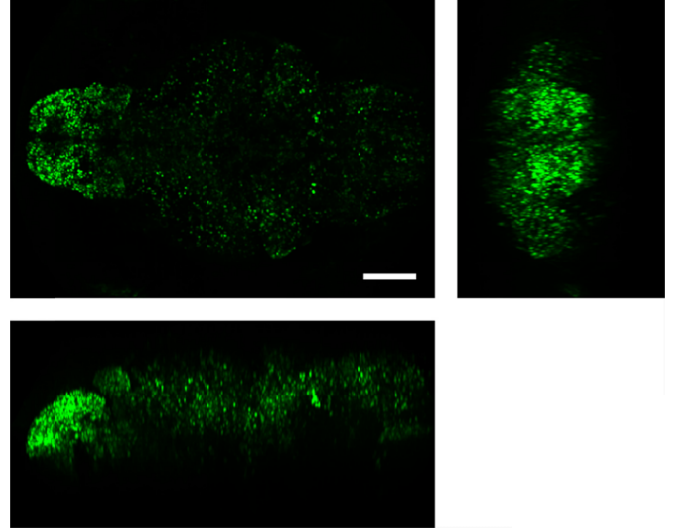


**Fig. S3.** Temporal maximum intensity projection (MIP) of reconstructed SDLFM volumes of larval zebrafish brain expressing pan-neuronal nuclear localized GCaMP6s. Top left, axial projection. Top right, rostral-caudal projection. Bottom, lateral projection. Scale bar, 100  $\mu\text{m}$ .

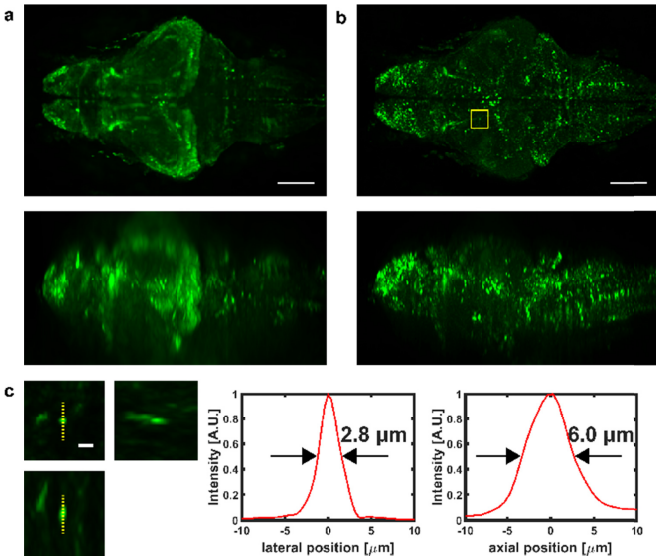


**Fig. S2.** (a) Temporal maximum intensity projections (MIPs) (top, axial projection; bottom, lateral projection) of reconstructed XLFM images of larval zebrafish brain expressing GCaMP6f. Scale bar, 100 $\mu\text{m}$ . (b) Temporal MIPs of reconstructed SDLFM images of larval zebrafish brain expressing GCaMP6f. Yellow boxed region was used to measure

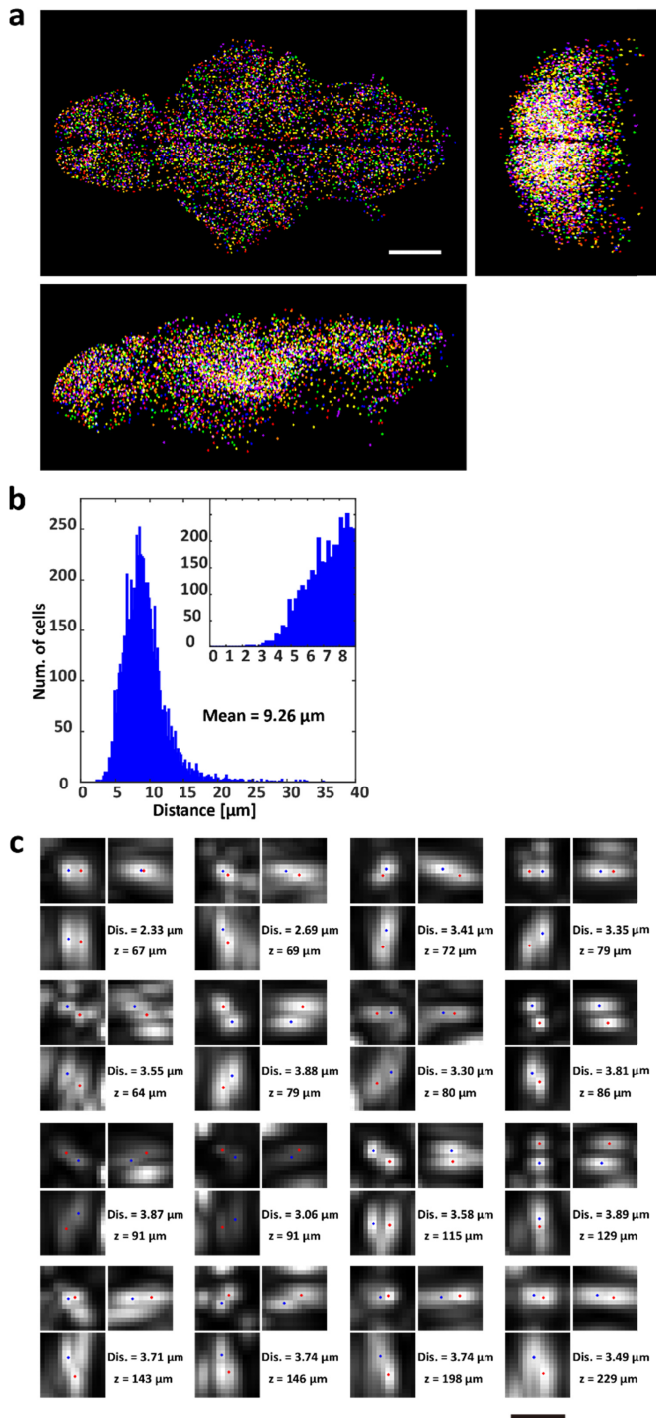


**Fig. S4.** (a) Spatial filters obtained from imaging of the larval zebrafish brain shown in Fig. 3b with SDLFM by directly segmenting the reconstructed volume without relying on signal extraction methods such as nonnegative matrix factorization. Random colors are assigned to each spatial filter. Top left, axial projection. Top right, rostral-caudal projection. Bottom, lateral projection. Scale bar, 100  $\mu\text{m}$ . (b) Histogram of the distances between individual cells and their nearest neighbor cells in **a**. Sub-pixel-precision cell centers were calculated using 3-D Gaussian fitting. (c) MIPs of example neuron pairs that were less than 4  $\mu\text{m}$  apart from each other at various depths below the brain surface. Top left, axial projection. Top right, rostral-caudal projection. Bottom, lateral projection. Scale bar, 10  $\mu\text{m}$ .



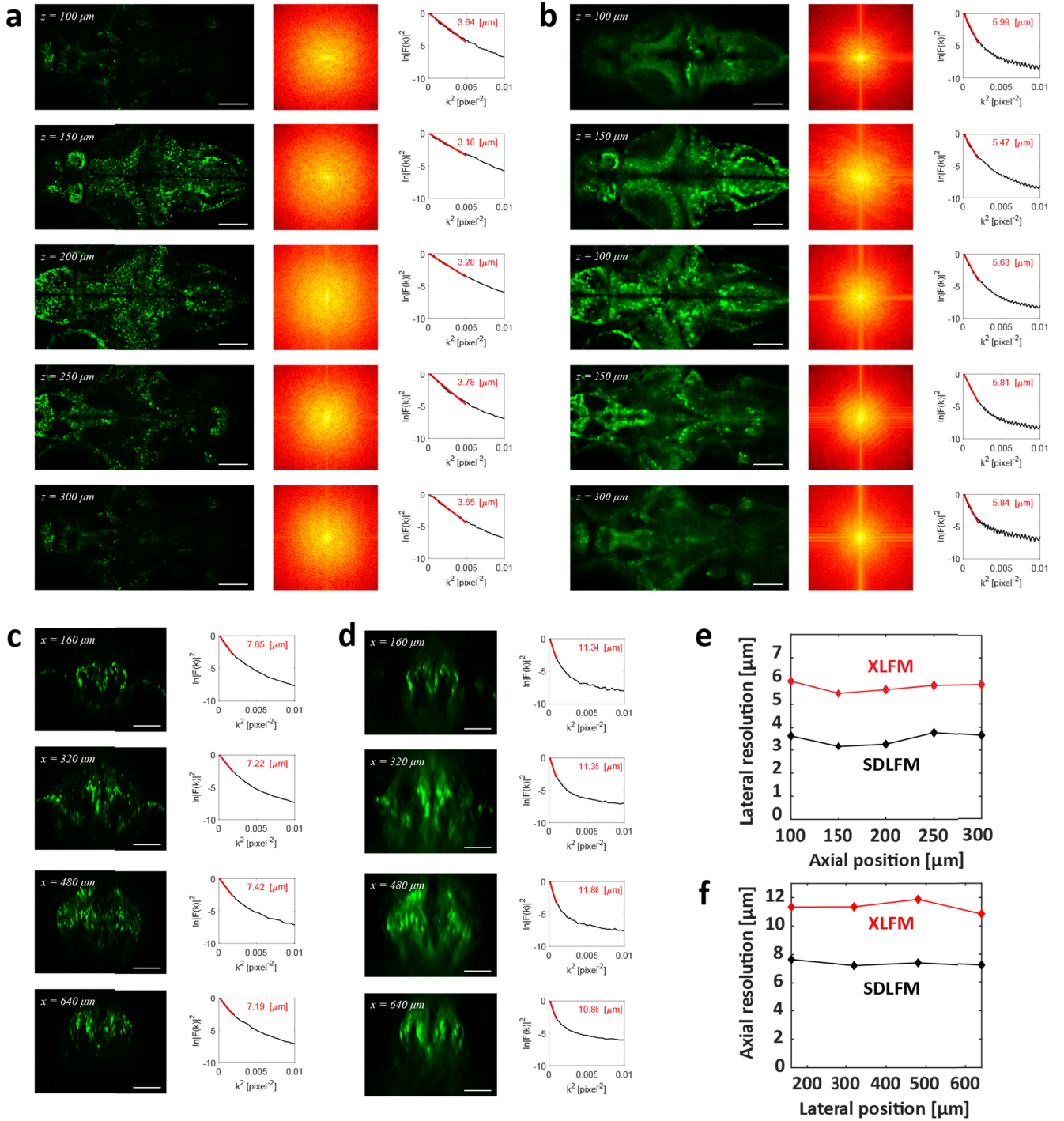


**Fig. S5.** Resolution estimation of SDLFM and XLFM in pan-neuronal NLS-GCaMP zebrafish brain using Fourier domain analysis. (a) Lateral resolution estimation of SDLFM at different depths using 2-D Fourier domain analysis. Z-slices (left) of the temporal MIP of 3-D images. Z indicates the depth from the top surface of the brain. Fourier transforms of z-slices (center). The lateral resolution was estimated (right) by measuring the slope of the red line fit to the left end of the black line which was obtained from the radial average of the magnitude of the 2-D Fourier transform of the image. Scale bar, 100  $\mu\text{m}$ . (b) Lateral resolution estimation of XLFM at different depths using 2-D Fourier domain analysis. As in a. Scale bar, 100  $\mu\text{m}$ . (c) Axial resolution estimation of SDLFM at different lateral positions using 1-D Fourier domain analysis. X-slices (left) of the temporal MIP of 3-D images. X indicates the distance from the rostral edge of the brain. The axial resolution (right) was estimated by measuring the slope of the red line fit to the left end of the black line which was obtained from the average of the magnitude of the 1-D Fourier transforms of the image along the axial direction. Scale bar, 100  $\mu\text{m}$ . (d) Axial resolution estimation of XLFM at different lateral positions using 1-D Fourier domain analysis. As in c. Scale bar, 100  $\mu\text{m}$ . (e) Measured lateral resolution of XLFM and SDLFM along the z-axis. (f) Measured axial resolution of XLFM and SDLFM along the x-axis.

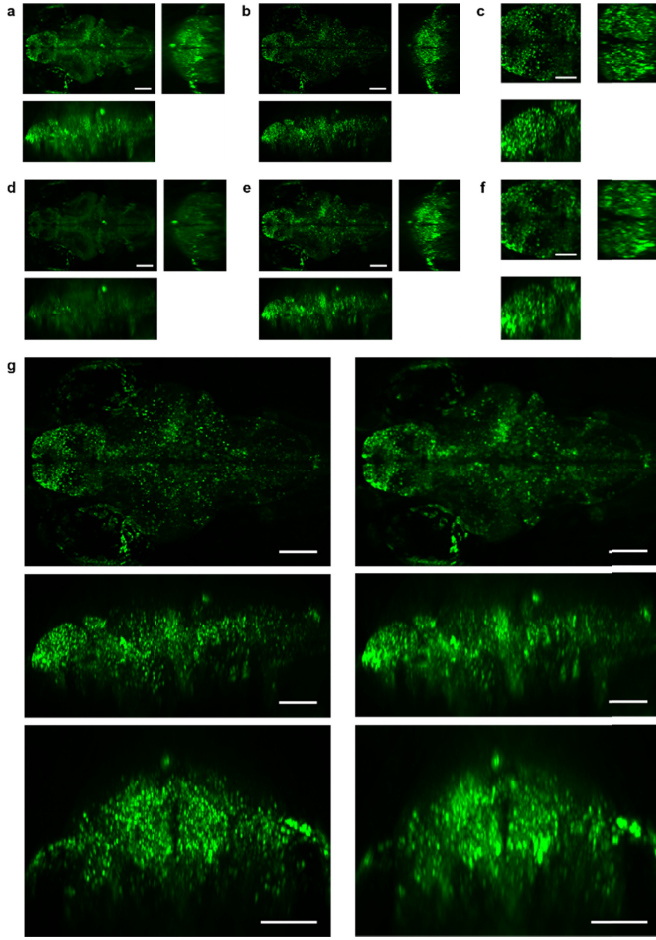


**Fig. S6.** (a) Temporal MIP of conventional XLFM volume reconstruction of larval zebrafish brain expressing NLS-GCaMP6s pan-neuronally. Top left, axial projection. Top right, rostral-caudal projection. Bottom, lateral projection. Same panel organization shown in **b-f**. Scale bar: 100  $\mu\text{m}$ . (b) Temporal MIP of SDLFM reconstruction of the sparse component. From the same raw data as in **a**. Scale bar: 100  $\mu\text{m}$ . (c) Zoomed-in image of the forebrain in **b**. Scale bar: 50  $\mu\text{m}$ . (d) Temporal MIP of volume reconstruction of the low rank component. From the same raw data as in **a**. Scale bar: 100  $\mu\text{m}$ . (e) Temporal MIP of the volume acquired by subtracting the volume from the low rank component as in **c**. From the conventional XLFM volume as in **a**. Scale bar: 100  $\mu\text{m}$ . (f) Zoomed-in image of the forebrain in **e**. Scale bar: 50  $\mu\text{m}$ . (g) Side-by-side comparisons of the temporal MIP along z, x, y axes, respectively. Top, axial projection. Middle, lateral projection. Bottom, rostral-caudal projection. Scale bar: 100  $\mu\text{m}$ .

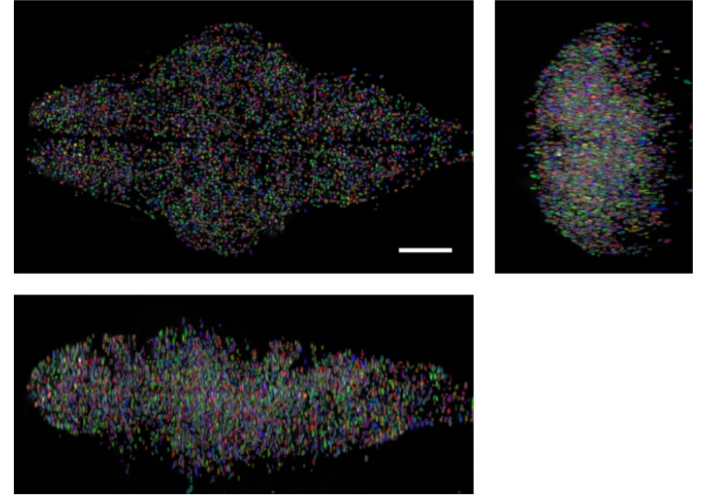


**Fig. S7.** Spatial filters obtained from imaging larval zebrafish brain expressing pan-neuronal GCaMP6f with SDLFM by directly segmenting the reconstructed volume without relying on signal extraction methods such as nonnegative matrix factorization. Random colors are assigned to each spatial filter. Top left, axial projection. Top right, rostral-caudal projection. Bottom, lateral projection. Scale bar, 100  $\mu\text{m}$ .

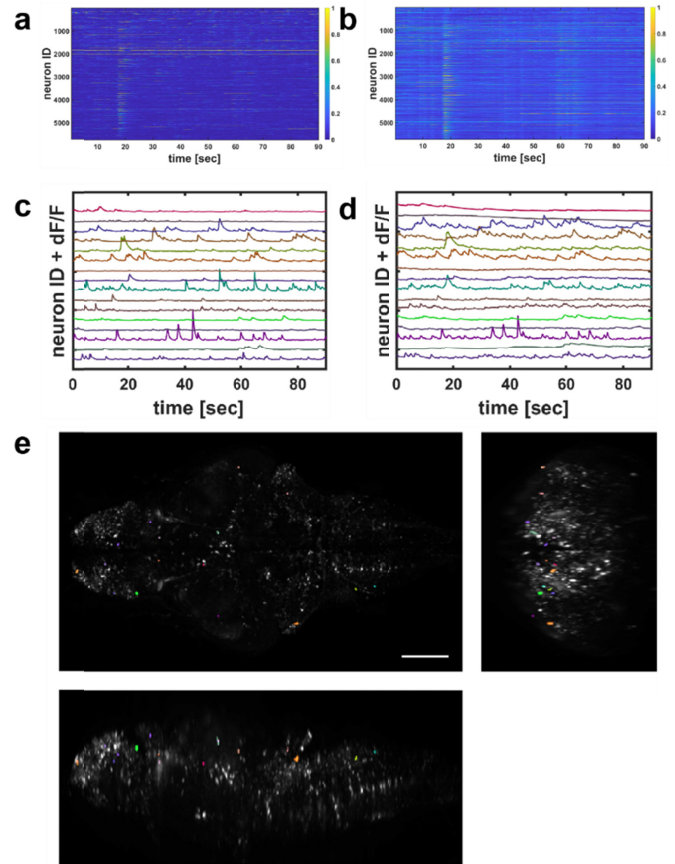


**Fig. S8.** (a) Extracted neuronal activities from imaging larval zebrafish brain expressing pan-neuronal GCaMP6f with SDLFM shown as a heat map. (b) Extracted neuronal activities from imaging larval zebrafish brain expressing pan-neuronal GCaMP6f with XLFM shown as a heat map. From the same raw data as in **a**. (c) Signal traces of the extracted neuronal activities from randomly selected neurons with SDLFM. (d) Signal traces of the extracted neuronal activities from randomly selected neurons with XLFM. (e) Side-by-side comparisons of the extracted neuronal activities along z, x, y axes, respectively. Top, axial projection. Middle, lateral projection. Bottom, rostral-caudal projection. Scale bars: 100  $\mu\text{m}$ .

SDLFM. (d) Signal traces of the extracted neuronal activities from randomly selected neurons with XLFM. From the same raw data as in **c**. (e) Overlay of the maximum intensity projection of the reconstructed volume with the spatial filters that correspond to the randomly selected neurons in **c** and **d**. Color of each spatial filter is matched that of the corresponding signal trace. Top left, axial projection. Top right, rostral-caudal projection. Bottom, lateral projection. Scale bar, 100 $\mu$ m.

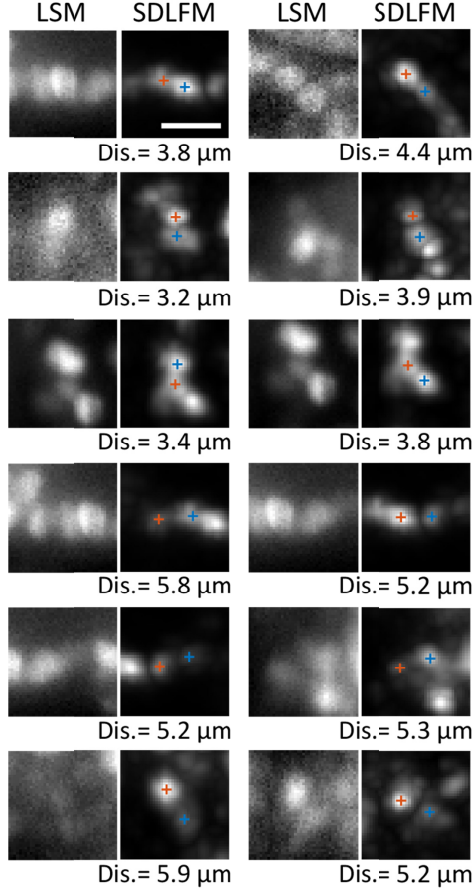


**Fig. S9.** Example resolved neuron pairs from rapid-alternation LSM/SDLFM imaging of a larval zebrafish brain expressing NLS-GCaMP6. These zoomed-in z-slices (70  $\mu$ m below the brain top surface) were cropped from the images shown in Figure 4c. Cell-to-cell distances were measured between the cell centers. Scale bar, 10  $\mu$ m.

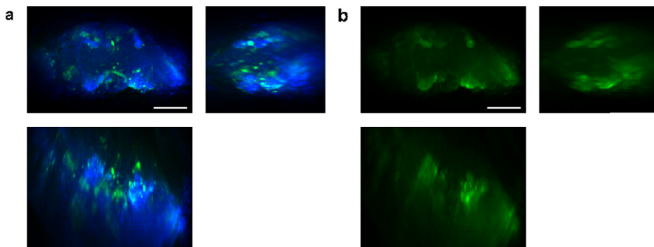


**Fig. S10.** (a) Temporal MIP of reconstructed SDLFM images of adult Drosophila brain expressing GCaMP6s. The low rank component and the sparse component are shown as blue and green, respectively. Top left, axial projection. Top right, lateral projection. Bottom, rostral-caudal projection. Scale bar, 100 $\mu$ m. (b) Temporal MIP of reconstructed XLFM images of adult Drosophila brain expressing GCaMP6s. From the same raw data as in **a**. Scale bar, 100 $\mu$ m.

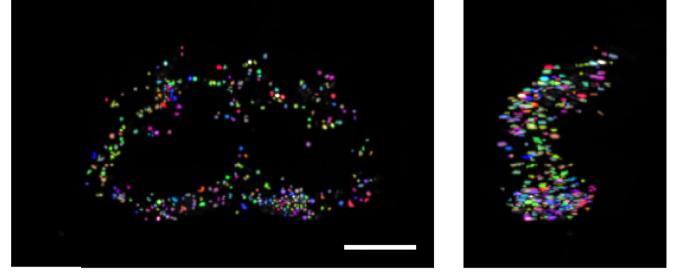


**Fig. S11.** Spatial filters obtained from imaging adult Drosophila brain expressing pan-neuronal NLS-GCaMP6m with SDLFM by directly segmenting the reconstructed volume. Random colors are assigned to each spatial filter. Top left, axial projection. Top right, lateral projection. Bottom, rostral-caudal projection. Scale bar, 100  $\mu$ m.

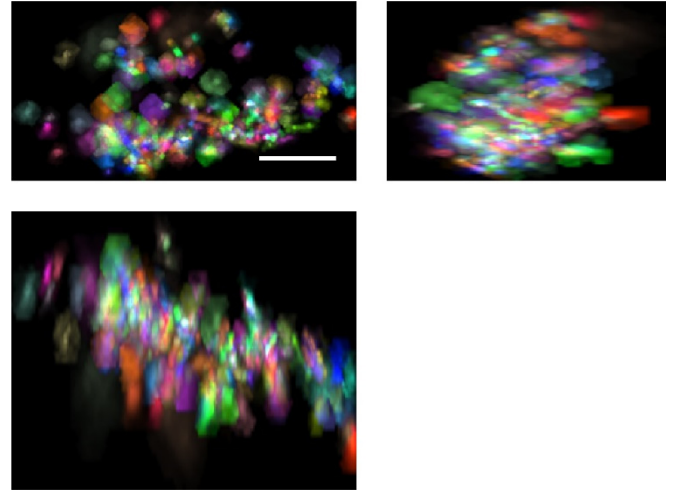


**Fig. S12.** Spatial filters obtained from the Drosophila whole brain recording by applying C-NMF to the reconstructed 4-D SDLFM data set. Random colors are assigned to each spatial filter. Top left, axial projection. Top right, lateral projection. Bottom, rostral-caudal projection. Scale bar, 100  $\mu$ m.



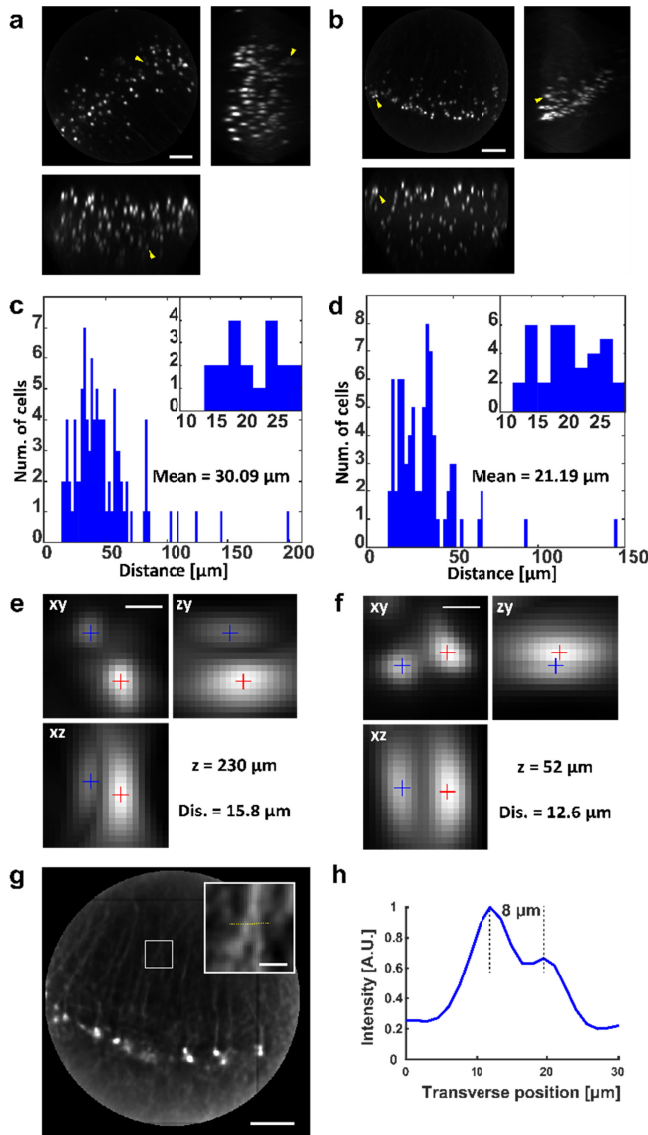


**Fig. S13.** We performed XLFM imaging of a 500-μm-thick mouse brain slice of cortex (layer 2/3) expressing YFP (Thy1-YFP) to experimentally verify the performance of our system when the sample is scattering and sparsely labeled (which provides an estimate of achievable resolution with SDLFM). We were able to confirm that our system can image as deep as 300 μm. (a,b) Maximum intensity projections of 3-D reconstructed volumes from imaging 500-μm-thick live mouse brain slices of cortex expressing YFP (Thy1-YFP) using XLFM demonstrating its capability to image scattering tissue. The diameter of the field-of-view circle is ~700 μm. Top left, axial projection. Top right and bottom, lateral projections. Scale bar: 100 μm. (c) Histogram of the center-to-center distances between individual cells and their nearest neighbor cells in **a**. (d) Histogram of the center-to-center distances between individual cells and their nearest neighbor cells in **b**. (e) 3-D max intensity projections of an example cell pair 230 μm underneath the sample surface in **a** (yellow arrow). Gaussian-filter-fitted cell centers are marked with '+' signs. Z indicates the imaging depth from the top sample surface. X and Y are the lateral coordinates within a z-slice. Scale bar: 10 μm. (f) 3-D max intensity projections of an example cell pair 52 μm underneath the sample surface in **b** (yellow arrow). Gaussian-filter-fitted cell centers are marked with '+' signs. Scale bar: 10 μm. (g) A z-slice from **b**. The z-slice was 100 μm below the brain slice surface which was determined as the first z-slice with a neuronal cell body. The inset in upper right zooms in

on the white box. Scale bar, 20 μm. (h) The transverse intensity profile across the yellow dashed line in **g**. Putative dendritic processes that were separated by 8 μm were resolved.

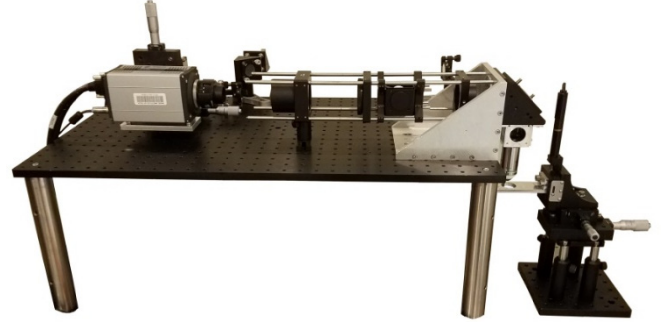


**Fig. S14.** Photograph of the XLFM used as the hardware of SDLFM.

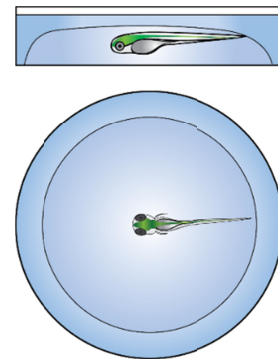


**Fig. S15.** Illustration of zebrafish preparation for imaging. A larval fish is embedded in agar in a Petri dish and water is added.

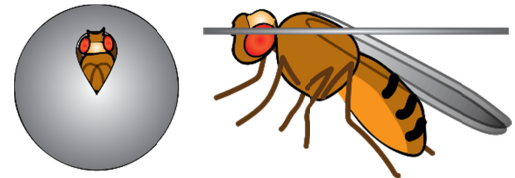


**Fig. S16.** Illustration of Drosophila preparation for imaging. An adult fly is mounted on a custom designed mount (thin metal sheet with a hole) and immobilized. The cuticle and the tissue above the brain are removed for imaging.

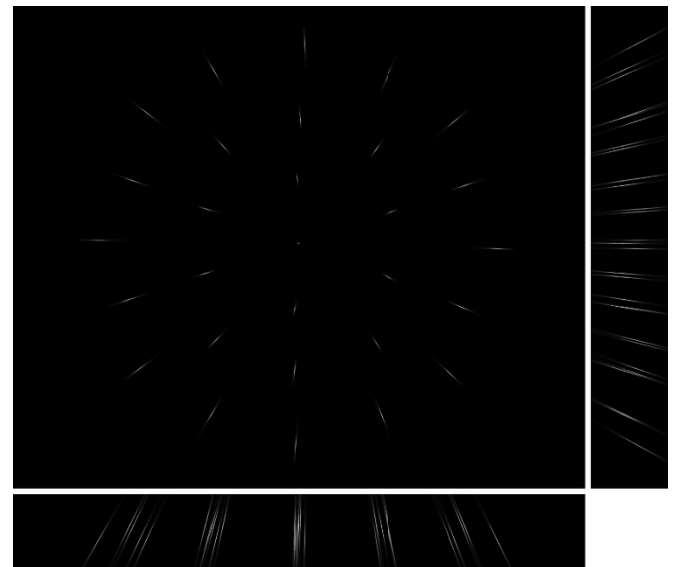




**Fig. S17.** Empirical PSF of the XLFM obtained by taking a z-stack image of a green fluorescent bead with 1 $\mu$ m diameter with 2.5 $\mu$ m z-step size. Top left, axial projection. Top right and bottom, lateral projections.

**Table S1. System design**

	Objective lens	Relay lens 1	Relay lens 2	Microlens	Camera
XLFM1	16x 0.8NA water dipping objective lens (CFI75 LWD 16xW, Nikon)	f=180mm achromatic doublet (AC508-180-A-ML, Thorlabs)	f=125mm achromatic doublet (PAC074, Newport)	f=36.1mm plano-convex axial position offset = 0.5mm 29 lenses in total	Andor Zyla 5.5
XLFM2 & hybrid LSM- SDLFM				f1=36.6mm f2=35.4mm plano-convex axial position offset = 0mm 29 lenses in total	Andor Zyla 5.5
XLFM3				f1=36.6mm f2=35.4mm plano-convex axial position offset = 0mm 19 lenses in total	Hamamatsu Orca Flash 4.0 v3

**Table S2. Simulation parameters**

Parameters	Value
number of neurons	80,000
size of neurons (radius)	2 [ $\mu$ m] – 2.5 [ $\mu$ m]
spatial distribution of neurons	A sphere was randomly generated within the volume predefined by a fish brain shaped mask. The sphere was accepted as a neuron if it does not spatially overlap with any existing neuron. This process was repeated until the target number of neurons was reached.
average distance from a cell to the nearest cell (center-to-center)	5.54 [ $\mu$ m]
rise time (GCaMP)	45 [msec]
decay time constant (GCaMP)	142 [msec]
dF/F <sub>0</sub> (GCaMP)	0.3
(F <sub>0</sub> : baseline fluorescence)	
cell-to-cell brightness variation (GCaMP)	50%
synchronicity	6.25%, 12.5%, 25%, 50%, 100%
average effective firing rate	0.2 Hz, 0.4 Hz, 0.8 Hz, 1.75 Hz, 20 Hz
frame rate	20 [Hz]
read noise (s.t.d. level relative to the brightest pixel value)	0.1%
shot noise (number of the expected shot noise, $\sqrt{N}$ , at the brightest pixel)	100 e <sup>-</sup>
optical configuration	Objective lens: 16x 0.8NA Microlens array focal length = 36.1mm Relay lens 1 focal length = 180mm Relay lens 2 focal length = 125mm Pixel size = 6.5 $\mu$ m Number of pixels = 2160 $\times$ 2560 (embedded in the point spread function by using an empirical PSF of XLFM1)

**Table S3. System-data correspondence**

System	Data
XLFM1	Fig. 3, Fig. S1, Fig. S4, Fig. S5, Fig. S6, Fig. S7, Fig. S16, Media S1, Media S2, Media S4, Media S5
XLFM2	Fig. S2, Fig. S9, Media S3, Media S6, Media S7
XLFM3	Fig. 5, Fig. S10, Fig. S11, Fig. S12, Media S9, Media S10, Media S11, Media S12, Media S13
hybrid LSM-SDLFM	Fig. 4, Fig. S8, Media S8

**Media S1.** XLFM whole brain functional imaging of a zebrafish larva expressing nuclear localized GCaMP6s pan-neuronally. Maximum intensity projection with rotating view. The data was acquired at a volume rate of 10 Hz.

**Media S2.** XLFM whole brain functional imaging of a zebrafish larva expressing GCaMP6f pan-neuronally. Maximum intensity projection with rotating view. The data was acquired at a volume rate of 10 Hz.

**Media S3.** SDLFM whole brain functional imaging of a zebrafish larva expressing nuclear localized GCaMP6s pan-neuronally. Maximum intensity projection with rotating view. The data was acquired at a volume rate of 2Hz. Temporal MIP is shown at the beginning.

**Media S4.** SDLFM whole brain functional imaging of a zebrafish larva expressing nuclear localized GCaMP6s pan-neuronally. Maximum intensity projection with rotating view. The data was acquired at a volume rate of 5 Hz. Temporal MIP is shown at the beginning.

**Media S5.** SDLFM whole brain functional imaging of a zebrafish larva expressing GCaMP6f pan-neuronally. Maximum intensity projection with rotating view. The data was acquired at a volume rate of 10 Hz. Temporal MIP is shown at the beginning.

**Media S6.** SDLFM whole brain functional imaging of a zebrafish larva expressing GCaMP6f pan-neuronally. Maximum intensity projection with rotating view. The data was acquired at a volume rate of 50 Hz. Temporal MIP is shown at the beginning.

**Media S7.** SDLFM whole brain functional imaging of a zebrafish larva expressing GCaMP6f pan-neuronally. Maximum intensity projection with rotating view. The data was acquired at a volume rate of 50 Hz. Temporal MIP is shown at the beginning.

**Media S8.** Rapidly alternating whole brain functional imaging of a zebrafish larva expressing nuclear localized GCaMP6s pan-neuronally using LSM (left) with a laser light sheet illumination and SDLFM (right) with a LED wide-field illumination to demonstrate the achievable resolution. The data was acquired at 5 Hz.

**Media S9.** SDLFM whole brain in vivo functional imaging of an adult *Drosophila* expressing NLS-GCaMP6m pan-neuronally. Maximum intensity projection with rotating view. The data was acquired at a volume rate of 5 Hz. SDLFM reconstruction (green) is overlaid on the volume-reconstructed low rank component (blue). Temporal MIP is shown at the beginning.

**Media S10.** SDLFM whole brain functional imaging of an adult *Drosophila* expressing GCaMP6s pan-neuronally. Maximum intensity projection with rotating view. The data was acquired at a volume rate of 2 Hz. SDLFM reconstruction (green) is overlaid on the volume-reconstructed low rank component (blue).

**Media S11.** SDLFM whole brain functional imaging of an adult *Drosophila* expressing GCaMP6s pan-neuronally. Maximum intensity projection with rotating view. The data was acquired at a volume rate of 10 Hz. SDLFM reconstruction (green) is overlaid on the volume-reconstructed low rank component (blue).

**Media S12.** SDLFM whole brain functional imaging of an adult *Drosophila* expressing GCaMP6s pan-neuronally. Maximum intensity projection with rotating view. The data was acquired at a volume rate of 5 Hz. SDLFM reconstruction (green) is overlaid on the volume-reconstructed low rank component (blue).

**Media S13.** SDLFM whole brain functional imaging of a zebrafish larva expressing nuclear localized GCaMP6s pan-neuronally. Maximum intensity projection with a fixed view. The data was acquired at a volume rate of 10 Hz. Temporal MIP is shown at the beginning.

**Code 1.** SDLFM software for sparse decomposition and volume reconstruction written in MATLAB.

## References

1. Jacques, S. L., Optical properties of biological tissues: a review. *Physics in Medicine and Biology* 58 (2013).